Oceanic Fronts in the Northern South China Sea

14

Quran Wu[*,†], Hongyang Lin[*,‡] and Jianyu Hu[*]

[*] *State Key Laboratory of Marine Environmental Science, College of Ocean and Earth Sciences, Xiamen University, Xiamen, Fujian, China*
[†] *National Centre for Atmospheric Science, University of Reading, Reading, UK*
[‡] *hylin@xmu.edu.cn*

A front is a narrow transition zone that separates water masses of distinct properties. It is a common feature in marginal seas and world oceans, and has important implications for marine ecosystems. Northern South China Sea (NSCS) features a long front band spanning from the Hainan Island to the Taiwan Strait. Substantial progress has been made regarding the investigations into this front band since the 2000s. Representative studies are reviewed in this chapter. Starting from the southern end, it is found that both Chl-a and SST fronts are observed around the Hainan Island, with the former being strongly affected by tidal mixing. Moving to the center of the front band, a statistical modeling approach reveals that SST fronts of 10–50 km width separate water masses that differ in temperature at 3.5–4.5°C along the Guangdong coast. The northern part of the front band is occupied by fronts in the Taiwan Strait with distinctive seasonality. During winter, coastal water and intrusion of open ocean water interleave each other in the center of the strait, resulting in complex geometry of frontal features. During summer, SST fronts are identified in the Taiwan Bank, the Pearl River plume extension region, and the coastal upwelling region southwest of the strait. Their surface temperature and salinity signatures are examined using *in situ* observations.

14.1 Introduction

Oceanic fronts are regions of enhanced horizontal gradients of seawater properties (temperature, salinity, density, etc.) that separate water masses of distinct origins. For example, thermal fronts are narrow transition zones between water masses of different temperature signatures and normally characterized by enhanced sea surface temperature (SST) gradients. Thermal fronts exhibit diverse spatiotemporal signatures, with length scales from meters to thousands of kilometers and persistent time from days to years. SST gradients in a strong thermal front have a typical order of 0.1–1°C/km [Belkin *et al.*, 2009].

Oceanic fronts and frontal processes play important roles in marine ecosystems. In surface convergent fronts, ocean currents aggregate plankton leading to elevated rate of primary production [Lohmann and Belkin, 2014]. In the subsurface, front-induced circulation (via instability processes) tends to restratify upper oceans, which facilitates phytoplankton blooms during spring in high latitudes [Taylor and Ferrari, 2011]. Strong geostrophic currents are observed along density fronts, which affect exchanges of heat, freshwater and nutrients between different regions. In high latitude outcrop regions, fronts are pathways or "windows" through which the surface ocean communicates with the ocean interior, and thus affect the formation of various water masses as well as their associated ecosystems [Ferrari, 2011].

Fronts of different properties are typically collocated, although some spatial offsets are expected. For example, a river plume front can be defined via either its temperature or salinity signatures. Considering that remote sensing SST data have longer time series (dating back to 1982) and better spatial coverage than other surface ocean variables (e.g., salinity and chlorophyll), SST front is the most common metric used to map activities of oceanic fronts in the literature.

In the northern South China Sea (NSCS), the most prominent frontal feature is the long front band along the coast of the mainland China, ranging from the Taiwan Strait in the north to the Beibu Gulf in the south. Wang *et al.* [2001] suggested that this long front band is formed as a boundary between the relatively cold coastal water and the relatively warm South China Sea (SCS) open water. It is strongest during winter due to the northeasterly monsoon, which pushes the two water masses together, but weakest during summer as the monsoon reverses. Wang [2004] pointed out that the strength of fronts in the NSCS is affected by strength of the northeasterly monsoon as well as the Kuroshio intrusion. Instability analysis based on an

idealized setup was carried out by Wang [2004] to investigate the roles of baroclinic and barotropic processes in generating frontal instabilities. Using *in situ* data, Jing *et al*. [2015] revealed that the summertime SST front east of the Hainan Island is due to upwelled cold water from outer shelf driven by southwesterly monsoon. Strong seasonality is identified for fronts along Guangdong coast as well, and correlated with seasonal reversal of monsoon [Qiu *et al*., 2017]. They suggested that sensible heat flux contributes to the formation and decaying of fronts in that region. Frontal regions often feature complex 3D circulation. This was captured by Xie *et al*. [2017] in their diagnoses of *in situ* data, with roles of different terms in the omega equation being quantified.

This chapter reviews several representative studies regarding the long front band along mainland China. Starting from its southern end, we first review the study of SST and Chl-a fronts around the Hainan Island by Hu *et al*. [2003]. Then, we describe the Guangdong coastal fronts, located in the middle of the long front band, by using Wu *et al*.'s [2015] improved statistical front detection method. Moving northward, seasonal evolution of SST fronts in the Taiwan Strait is presented by reviewing Pi and Hu's [2010] work based on satellite SST data. We further introduce winter- and summer-time structures of fronts in the Taiwan Strait based on *in situ* studies of Li *et al*. [2006] and Zhang *et al*. [2014], respectively.

14.2 Chl-a and SST Fronts Around the Hainan Island

The Hainan Island is a big island located in the northwest of the SCS. It is separated from the Guangdong province via the Qiongzhou Strait on its north, and features a steep continental slope on its southeast. The Beibu Gulf is located to the west of the Hainan Island and has a maximum depth less than 80 m in most regions. SST fronts and Chl-a fronts had been observed around the Hainan Island in satellite remote sensing images [e.g., Wang *et al*., 2001; Tang *et al*., 2003], which are the southern part of the long front band along mainland China. It remains unclear what processes are responsible for generation of fronts in this region. Here, we summarize the work by Hu *et al.* [2003], in which they examined the role of tidal mixing in determining the position of fronts east of the Hainan Island and in the Beibu Gulf.

14.2.1 *Satellite observations*

Surface Chl-a distribution around the Hainan Island and in the Beibu Gulf is characterized by narrow bands of high Chl-a water along the coastal regions, and water with relatively low Chl-a concentration in the open ocean, as revealed in a snapshot of satellite images taken in August of 1999 (Figure 14.1(a)). Sharp Chl-a fronts are formed between the above two water masses, and they tend to follow the isobath in that region. Monthly mean maps suggest similar distribution of Chl-a in different seasons relative to that derived from the snapshot image, except during autumn and winter when the high Chl-a water in the Beibu Gulf extends offshore (Figure 14.2).

SST fronts are observed around the Hainan Island and in the Beibu Gulf during winter as evident in AVHRR-derived SST images (Figure 14.3). In the eastern coast of the Hainan Island and to the south of the Guangdong province, fronts tend to follow the 80 m isobath, where SSTs change from 21°C to 23°C within 10 km in the cross-front direction, featuring an SST gradient of 0.2°C/km. In the Beibu Gulf, fronts tend to follow the 40 m isobath, and are mostly confined in the north and northeast parts of the Gulf. During summer, most of SST fronts in that region disappear, as SSTs are warmer than 28°C in most regions homogeneously. The only exception is in the southeast of the Hainan Island, where near-shore SSTs remain low due to upwelled subsurface water. Spring and autumn are transitional seasons for SST fronts in this area, corresponding to the transition of the monsoon in the SCS.

14.2.2 *Roles of tidal mixing*

To investigate the role of tidal mixing in generating above fronts, Hu *et al.* [2003] used the Princeton Ocean Model (POM) to simulate major tidal components around the Hainan Island. The model domain is 105.5–128.5°E and 15.0–30.0°N, with a horizontal resolution of 1/12° (about 9.26 km) and seven vertical layers. To focus on the impact of tidal mixing, there is no wind stress, heat or freshwater flux being applied to the model, and the seawater temperature and salinity are set to constant values of 27°C and 34 PSU, respectively. Based on Hu *et al.* [2001], seven major tidal components, i.e., M_2, S_2, K_1, O_1, P_1, N_2 and K_2, are selected and then imposed to three open boundaries of the model domain, as follows:

$$\zeta = \sum f_c H_c \cos[\omega_c t + (V_{0c} + u_c) - g_c], \tag{14.1}$$

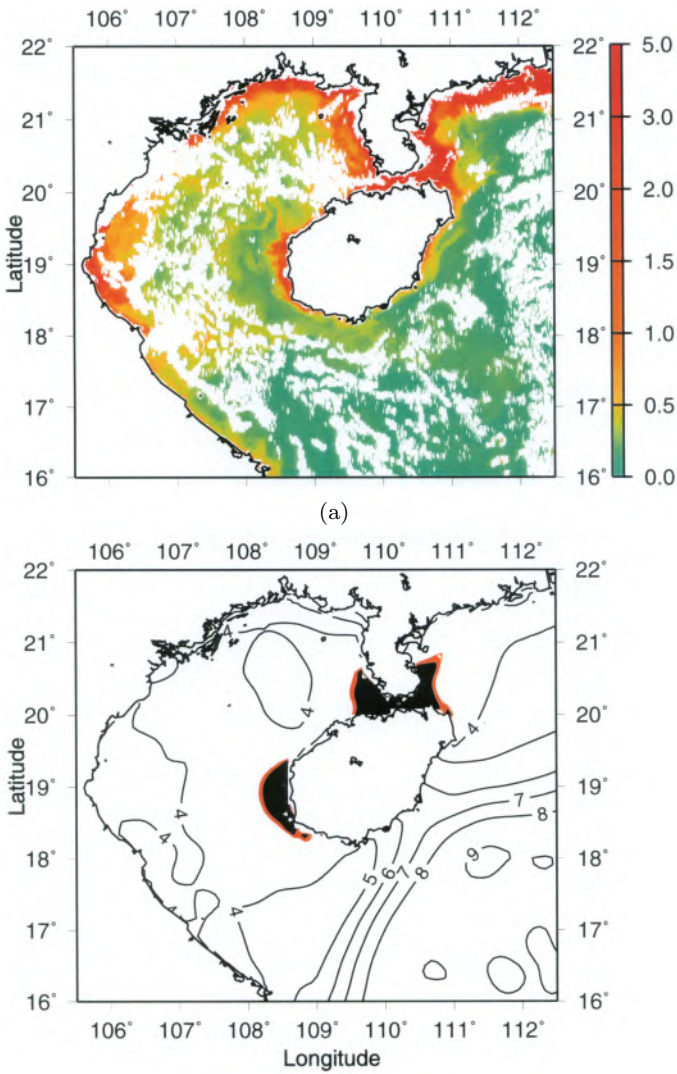

Fig. 14.1. (a) Snapshot cloud-free SeaWiFS-derived Chl-a image on 19 August 1999 and (b) log (h/u^3) contour lines in the studied area around the Hainan Island.

Notes: The unit of Chl-a concentration is in mg m^{-3} in (a), and the areas with the value of log (h/u^3) less than 2.9 are shaded in black color in (b).

Source: From Hu *et al.* [2003].

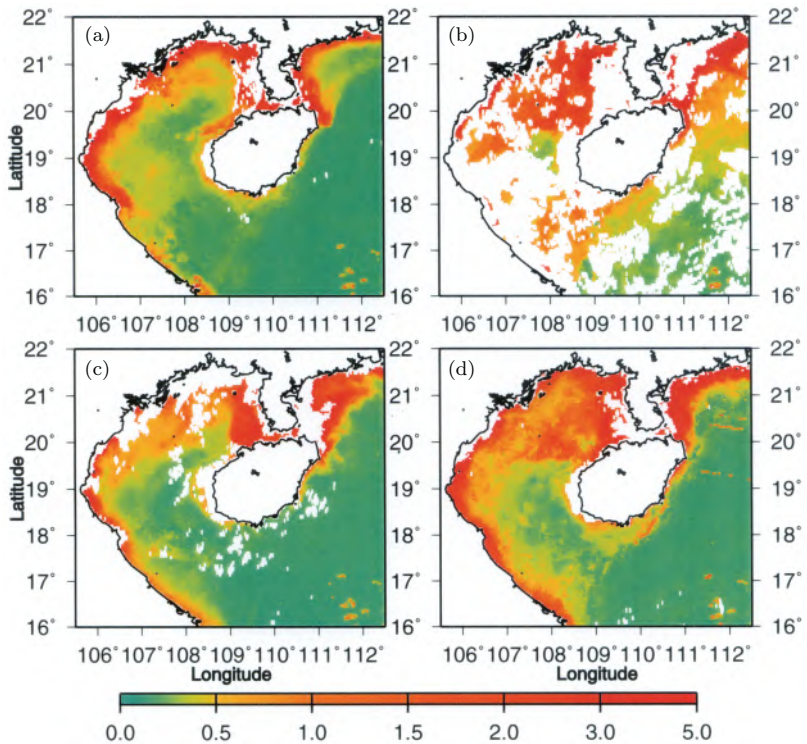

Fig. 14.2. Monthly mean SeaWiFS-derived Chl-a images. (a) August 2000, (b) December 2000, (c) April 2000 and (d) October 2000.

Notes: The unit of Chl-a concentration is in mg m^{-3}.

Source: From Hu *et al.* [2003].

where H_c and g_c are the harmonic constants of amplitude and phase, respectively, and the subscript c denotes different tidal components. The angular speed is ω_c, nodal factor, f_c, nodal angle, u_c and V_{0c}, the initial phase angle of the equilibrium tide. The parameters f_c, u_c and V_{0c} are calculated using astronomical constants. The harmonic constants H_c and g_c are derived from six years of TOPEX/Poseidon altimeter data [Hu *et al.*, 2001]. The cotidal charts generated from this model (not shown) agree well with those derived from satellite altimeter data [Yanagi *et al.*, 1997; Hu *et al.*, 2001], numerical models [Fang *et al.*, 1999] and *in situ* observations [Huang *et al.*, 1994].

The mean kinetic energy of the total seven tidal components simulated in the study area features high kinetic energy zones in the Qiongzhou

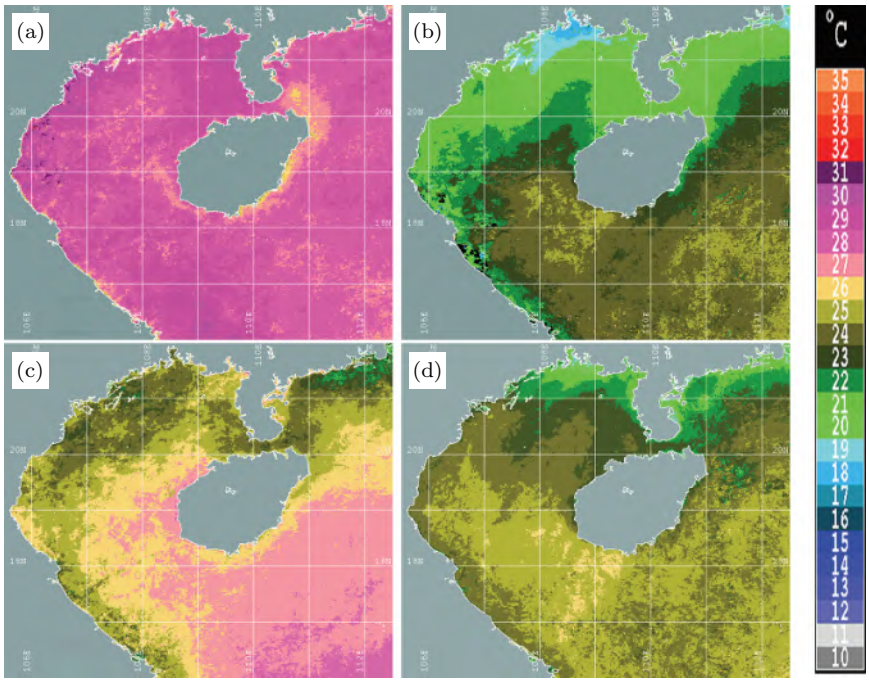

Fig. 14.3. Monthly mean AVHRR-derived SST images. (a) August 2000, (b) December 2000, (c) April 2000 and (d) November 2000.

Source: From Hu *et al.* [2003].

Strait ($>15 \times 10^{-2}\,m^2/s^2$) and to the southwest of the Hainan Island ($>8 \times 10^{-2}\,m^2/s^2$) (Figure 14.4). In contrast, there are low kinetic energy zones located to the southeast of the Hainan Island and in the continental shelf of the Beibu Gulf, with values as low as $1–2 \times 10^{-2}\,m^2/s^2$.

By taking into account the tidal mixing and the depth of water column together, Simpson and Hunter [1974] suggested that the distribution of $\log(h/u^3)$ can be used as an indicator for the positions of tidal mixing fronts. In $\log(h/u^3)$, h is the depth in m and u is the time average of depth-mean tidal current in m/s [Loder and Greenberg, 1986]. The 3.0 contour of $\log(h/u^3)$ is found around the Qiongzhou Strait and to the southwest of the Hainan Island, with the former colocated with Chl-a fronts identified from the monthly mean Chl-a images, suggesting the important role of tidal mixing in the formation of those Chl-a fronts (Figure 14.1(b)). For the southwest of the Hainan Island, although Chl-a fronts are lacking in the monthly mean images, the colocation between

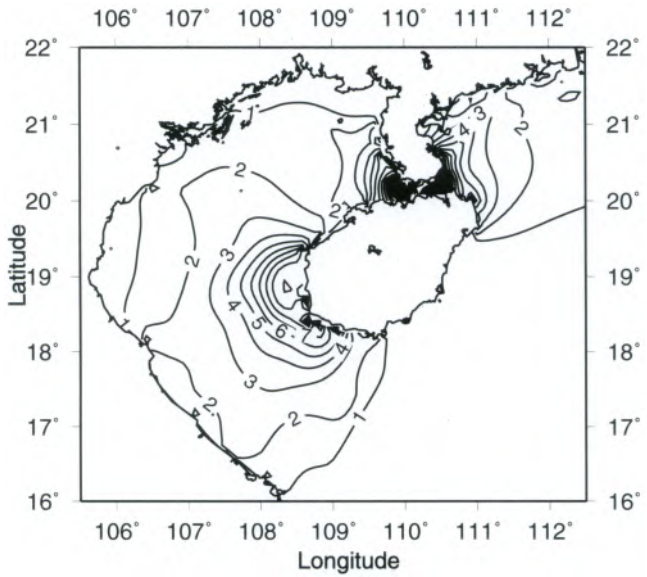

Fig. 14.4. Mean kinetic energy (10^2 m^2/s^2) in the studied area around the Hainan Island. *Source*: Taken from Hu *et al*. [2003].

Chl-a fronts and 3.0 contour of $\log(h/u^3)$ is observed in the snapshot image (Figure 14.1) clearly. Among the seven tidal components considered in this study, the M_2 and K_1 tides are more important than other components in determining the distribution of $\log(h/u^3)$ to the north of the Hainan Island.

Chl-a fronts are also identified along the coast of the north Beibu Gulf and the Vietnam coast (Figure 14.2), where the $\log(h/u^3)$ is higher than 3.0, suggesting weak tidal mixing in those regions (Figure 14.1(b)). As a result, it is likely that the high Chl-a water in the nearshore region is due to discharge of nutrients from rivers, rather than nutrients from lower layers induced by tidal mixing. SST fronts in the Beibu Gulf and around the Hainan Island are not aligned with the contours of $\log(h/u^3)$ in most regions (Figure 14.1(b)), and exhibit seasonal variations as revealed in the monthly mean SST images (Figure 14.3). This implies that processes such as surface heat fluxes and heat transport associated with coastal currents are more important than tidal mixing in the formation of SST fronts over those regions.

14.3 SST Fronts Along the Coast of Guangdong

This section reviews SST fronts in the central part of the long front band, i.e., along the coast of Guangdong, based on results from an improved statistical modeling approach [Wu *et al.*, 2015]. Most automatic front detection algorithms focus on edge features in SST images, including the histogram-based edge detection algorithm [Cayula and Cornilion, 1995; Hickox *et al.*, 2000], gradient-based algorithm [Wang *et al.*, 2001] and entropy-based edge detection algorithm [Vázquez *et al.*, 1999; Shimada *et al.*, 2005; Chang *et al.*, 2006]. A novel statistical modeling approach was proposed by Hopkins *et al.* [2010] to depict the spatiotemporal evolution of the whole frontal system, including both the narrow frontal zone and its adjacent water masses. Wu *et al.* [2015] improved and applied this method to the NSCS to derive the temperature range and width of SST fronts in that region.

14.3.1 *Statistical modeling approach to front detection*

A brief introduction of the statistical modeling method of Hopkins *et al.* [2010] is given here. To start with, a rectangular analysis window is set up to cover the frontal region, with a pair of its sides being perpendicular to the coastline. Define a Cartesian coordinate with x-axis being the alongshore direction and y-axis the cross-shore direction. The amplitude of SST is represented by the z-axis. Next, the idealized cross-front SST is defined as:

$$z_{\text{model}}(y) = \theta_1 + \theta_2 \tanh\left(\frac{y + \theta_4}{\theta_3}\right), \tag{14.2}$$

where $z_{\text{model}}(y)$ is SST (°C), θ_1 is mean SST of the front (°C), $2\theta_2$ is temperature range across the front (°C), $2\theta_3$ is width of the front (°), and $-\theta_4$ is the central position of the front (°). Assuming the difference between the idealized cross-front SST ($z_{\text{model}}(y)$) and the observed one ($z_{\text{rs}}(y)$) follows the normal distribution of $\phi(0, \sigma^2)$, the local likelihood function for observed cross-front SST can then be established. The Newton–Raphson algorithm is used to find an optimal set of parameters $\{\theta_1, \theta_2, \theta_3, \theta_4\}_{\text{opt}}$ which best fits $z_{\text{rs}}(y)$ onto $z_{\text{model}}(y)$. This parameter set is then used to quantify frontal features, and is hereafter referred to as frontal parameters.

Two deficiencies are identified when applying the statistical modeling method to detect SST fronts in the NSCS. First, the algorithm fails to solve

frontal features in some regions as it diverges. Second, non-frontal processes complicate the SST field in the NSCS, resulting in errors when estimating frontal parameters. In an attempt to address these two issues, Wu *et al.* [2015] introduced the genetic algorithm and an SST reconstruction algorithm to improve the performance of the statistical modeling method. The features of SST fronts captured by the improved algorithm will be discussed in the following.

14.3.2 *SST fronts detected using the improved statistical modeling method*

The improved statistical modeling method is applied to the NSCS to depict SST fronts there. The extraction window is set to be centered at 113.05°E and 21.2°N, with a length of 3° and a width of 1.4° (Figure 14.5, black rectangle). The angle between the length direction and meridians is 74°. Both satellite SST images and *in situ* data are used here. The satellite SST image is three day averaged over the period of 16–18 January 2010. The *in situ* data were collected during the cruise of January 2010. It includes

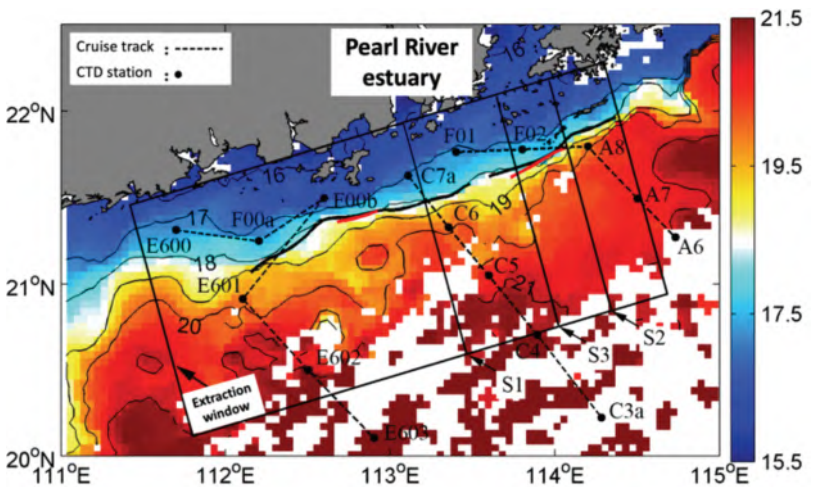

Fig. 14.5. SST (shading) averaged over 16–18 January 2010 and central positions of fronts detected by the statistical modeling method (solid lines).

Notes: The red and black solid lines are derived from the original and improved methods, respectively. The extraction window and transects of the January 2010 cruise are labeled in thin solid lines.

Source: From Wu *et al.* [2015].

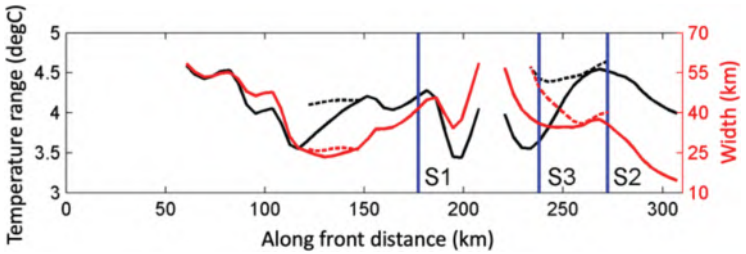

Fig. 14.6. Temperature range (black) and width (red) of fronts in Figure 14.5 as a function of along front distance (km). The dashed and solid lines correspond to results of original and improved statistical modeling methods.

Source: Taken from Wu *et al.* [2015].

three transects that are nearly perpendicular to SST fronts: C7a-C5-C3a (7–8 January), E601-E603 (9–10 January) and F01-A8-A6 (19–20 January) (labeled in Figure 14.5).

The SST fronts during 16–18 January in the study region are indicated by the convergence of 17–20°C SST contours in the remote sensing image (Figure 14.5). In addition to that, intrusion of warm water from open oceans is evident between 112°E and 114.2°E, complicating the cross-front SST distribution. This front is detected by both original and improved statistical modeling methods, though the frontal segment extracted by the improved method is longer than the original one by a factor of three as shown by the red and black lines in Figure 14.5. The temperature range across the front is between 3.5°C and 4.5°C (Figure 14.6, black lines), while the width of the front varies substantially, ranging from 10 to 50 km (Figure 14.6, red lines). The temperature range and width derived from the improved method (solid lines in Figure 14.6) tend to be smaller than those of the original method (dashed lines in Figure 14.6), because the improved method is less affected by the intrusion of warm water from open oceans.

In order to compare SST fronts detected from satellite images and those from *in situ* observations, the *in situ* SST data from the transect C7a-C4 and F01-A7 are projected onto the cross-front sections S1 and S2, respectively (S1 and S2 are labeled in Figure 14.5). No front is detected from the transect E601-E603, thus it is not included in the following analyses. In both sections, the idealized cross-front SST estimated via the statistical modeling method (Figure 14.7, black solid lines) agrees with the *in situ* data (Figure 14.7, blue solid lines) in general, except for two caveats. In section S1, the *in situ* SST (Figure 14.7(a), blue lines) is 2°C higher and exhibits 20 km shift in

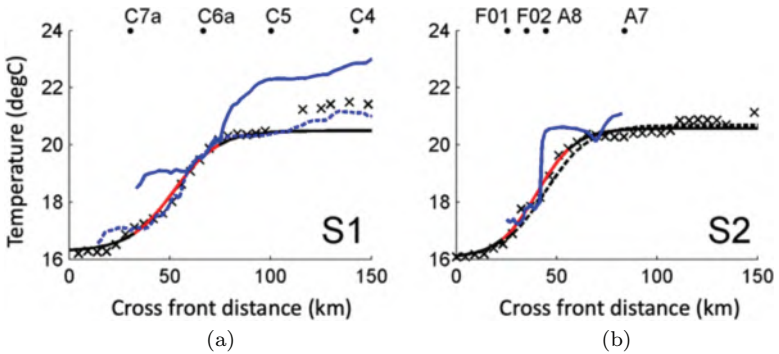

Fig. 14.7. *In situ* (blue solid lines) and remote sensing (crosses) SST along sections S1 (a) and S2 (b).

Notes: Positions of S1 and S2 are labeled in Figure 14.5. The black solid and dashed lines are idealized cross-front SST estimated from original and improved statistical modeling methods, respectively. In (a), the blue solid and dashed lines offset each other by 2°C and 20 km.

Source: From Wu *et al.* [2015].

the cross-front direction relative to the remote sensing one (Figure 14.7(a) crosses). This could result from 10-day time difference between the two datasets. In section S2, the *in situ* SST (Figure 14.7(b), blue lines) features much stronger cross-front temperature gradient than the remote sensing SST (Figure 14.7(b), crosses), probably due to low spatial resolution of the remote sensing data.

14.4 Seasonal Variation of SST Fronts in the Taiwan Strait

The Taiwan Strait is a narrow passage that connects the East China Sea and the SCS. Its circulation is strongly affected by seasonal monsoons, and the complex interactions among the low-salinity Zhemin coastal current, the intrusion of the Kuroshio and the SCS Warm Current. During the winter monsoon, the western part of the strait is dominated by the Zhemin coastal current, which brings cold and fresh water southward, while the eastern part of the strait is controlled by the northward-flowing SCS Warm Current. The convergence of different water masses leads to strong frontal activities in the Taiwan Strait during both winter and summer [e.g., Jan *et al.*, 2002; Chang *et al.*, 2006; Hu *et al.*, 2010].

In the Taiwan Strait, seasonal variation of SST fronts can be seen in satellite SST images averaged over seasons. The study by Pi and Hu [2010]

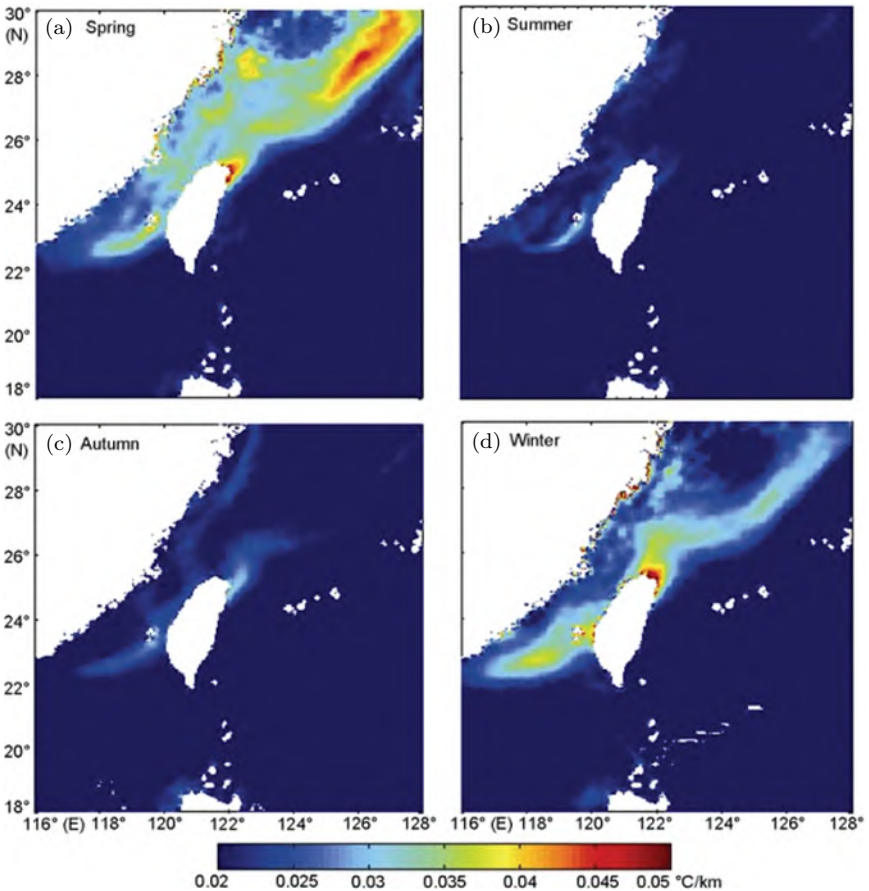

Fig. 14.8. Six-year mean of SST gradient magnitudes in different seasons for the study area. *Source*: From Pi and Hu [2010].

provided such an example (Figure 14.8). Specifically, the Taiwan Bank Front (TBF) features a banana shape distribution, with an average width of ∼50 km extending from the Taiwan Bank to the Penghu Channel. The Zhemin Coastal Front is claimed to have an "S" shape, possibly due to the interaction between the northward SCS Warm Current and the Kuroshio Branch intruding from the northeast of Taiwan. The "S" shape might be also associated with the offshore transport of the Zhemin Coastal Current as evidenced in Li *et al.* [2006]. The Zhang-Yun Ridge Front has a "C" shape, but is almost connected with the Zhemin Coastal Front. Pi and

Hu [2010] concluded that above SST fronts in the Taiwan Strait are stronger in spring and winter but weaker in summer, with autumn being their developing period.

14.5 SST Fronts in the Taiwan Strait during Winter–Spring: Fine Structures

In this section, we focus on wintertime fronts in the Taiwan Strait, by reviewing a five-day evolution of fronts [Li *et al*., 2006]. Note that a description of frontal features on such short time scale is very rare in the literature.

14.5.1 *Satellite observations*

High quality SST images of the Taiwan Strait are rare, especially during winter, due to heavy cloud coverage of that region. Li *et al.* [2006] selected two SST images in February 2001 and a sequence of three SST images in March 2001 after scanning the available SST images, to study the frontal evolution in the Taiwan Strait in winter and spring. The three subsequent SST images were obtained at 3:10 on 2 March (UTC), at 13:55 on 4 March and at 2:45 on 6 March, respectively (Figures 14.9(a)–14.9(c)). In the first image (Figure 14.9(a)), there is warm water intruding into the center of the strait, reaching as far as 25°N. The intrusion bifurcates into two branches: the west branch flowing towards the center of the strait and the east branch along the west coast of the Taiwan Island. Meanwhile, there is a cold water tongue that separates from the Fujian coast near the Pingtan Island and flows southward into the two branches of warm water. The SST difference between the warm and cold water tongues is about 6–8°C.

In the second image (Figure 14.9(b)) which was taken 60 h after the first one, more details of fronts are observed. The warm water intrusion has evolved into three branches. The west and east branches identified in the first image move further northeast, while a third branch is developing between them. The interleaving between different water masses leads to SST fronts with complex geometry. In the third image (Figure 14.9(c)) which was obtained 36 h after the second one, the frontal system continues to move northward as a whole. The west warm water branch appears to be pushed eastward as it meets the Zhemin coastal water, and the third branch has merged with the other two during that process.

Tracking the tip position of the west branch in the three images suggests that the frontal system migrates northward at 0.2 m/s between the

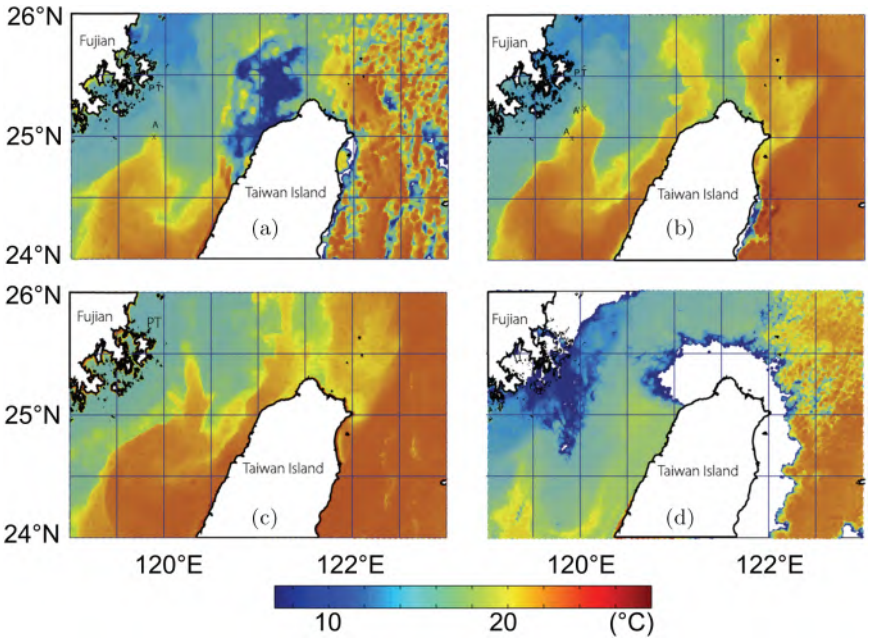

Fig. 14.9. SST observed by Moderate Resolution Imaging Spectroradiometer (MODIS) on board Satellite Terra. (a) 2 March 2001 (3:10 UTC); (b) 4 March 2001 (13:55 UTC); (c) 6 March 2001 (2:45 UTC); and (d) 16 February 2001 (3:00 UTC).

Source: From Li *et al.* [2006].

first two images, and 0.27–0.31 m/s between the second and third images. The two SST images of February are both contaminated with clouds. One is obtained on 18 February, which covers north of 24.8°N where no sign of warm water is identified. The other one is obtained on 16 February, and it shows that the warm water is about 1/3 into the strait from the south (Figure 14.9(d)).

14.5.2 *Vessel-based observations*

Similar large-scale frontal structures in the Taiwan Strait are also revealed by data from two vessel-based surveys during winter–spring. The first survey was conducted between 20 February and 8 March 1998, and it covers the Taiwan Strait with over 30 stations along three transects marked as T1, T2 and T3 in Figure 14.10. The surface temperature and salinity collected during the 1998 survey suggests northward and northwestward intrusions of warm and salty water (18–22°C, 33–34 PSU) in the eastern part of

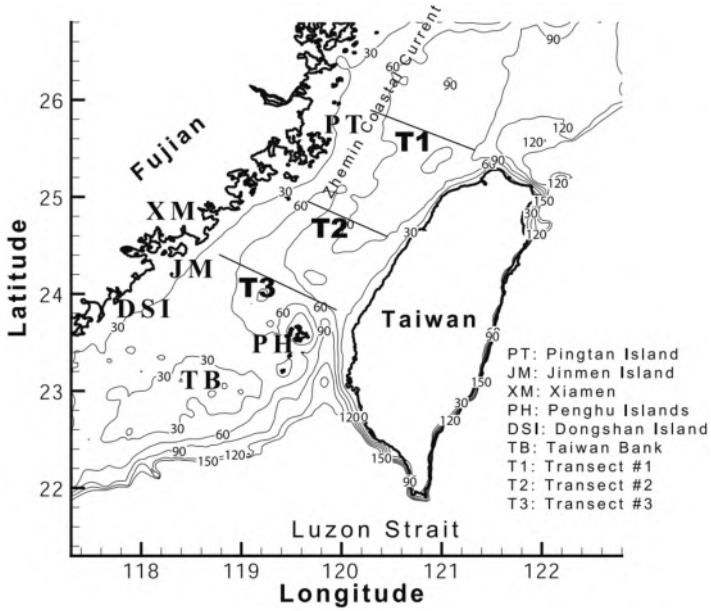

Fig. 14.10. Study area and transects of vessel-based survey during February–March 1998. *Source*: From Li *et al.* [2006].

the strait, and a southward intrusion of cold and fresh water (14–17°C, 30–32 PSU) in the western part of the strait (not shown). The cold and fresh water appears to be separated from the Zhemin coast around the Pingtan Island, suggesting that the Zhemin coastal current can enter the central Taiwan Strait. This is consistent with the evolution of SST from satellite images. The strength of surface temperature and salinity fronts can be as high as 1.2°C/km and 1.0 PSU/km, respectively.

The CTD profiles collected during the 1998 survey are used to illustrate vertical distributions of temperature and salinity underlying the surface fronts in the Taiwan Strait. It suggests much stronger temperature and salinity stratification on the west side of the strait than that on the east side, especially in transects T1 and T3 (Figure 14.11). The strong stratification on the west side is due to the contrast between the cold and fresh coastal water on the surface and the warm and salty water originated from open ocean, e.g., the Kuroshio intrusion. Since the coastal water is mostly confined to the west side of the strait, no such contrast is observed in the

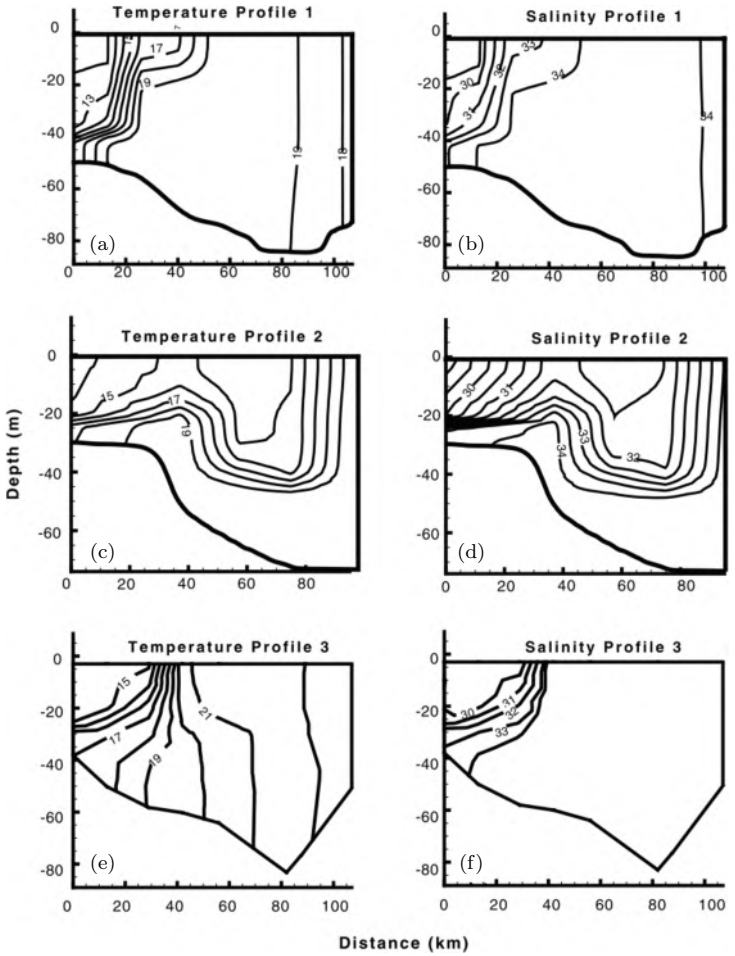

Fig. 14.11. Cross strait vertical profiles of temperature and salinity from the vessel-based survey during February–March 1998. (a) Temperature along transect 1, (b) salinity along transect 1, (c) temperature along transect 2, (d) salinity along transect 2, (e) temperature along transect 3 and (f) salinity along transect 3.

Notes: All transects are labeled in Figure 14.10.

Source: From Li *et al.* [2006].

east side of the strait. The second vessel-based survey was conducted during 20–25 March 2000, with a spatial coverage similar to the 1998 survey. It reveals surface temperature and salinity fronts on the west side of the Taiwan Strait as the 1998 survey, although the warm water intrusion and

the separation of the coastal current from the Zhemin coast are less evident (not shown).

14.6 SST and Salinity Fronts in the Southern Taiwan Strait in Summer

Summertime fronts in the southern Taiwan Strait are categorized into several segments based on their geographic locations or associated dynamic processes in Zhang *et al.* [2014], for example, the TBF, the Zhemin Coastal Front and the Zhang-Yun Ridge Front [Pi and Hu, 2010]. They tend to be weaker in summer and stronger in winter [Wang *et al.*, 2001; Pi and Hu, 2010]. Here, we summarize main findings of Zhang *et al.* [2014], who examined the summertime surface temperature and salinity signatures of those fronts.

14.6.1 *Taiwan Bank front (TBF)*

Due to the relatively large difference in water properties between the upwelled water around the Taiwan Bank and the ambient water, TBF is a strong front in the southern Taiwan Strait evident from both temperature and salinity. From south to north across the TBF, temperature first decreases from 29.3°C to 24.3°C (gradient is 0.63°C/km over the first 8 km) and then increases slowly to 28.5°C (gradient is 0.11°C/km over the next 39 km; see [Zhang *et al.*, 2014; Figure 4]). Salinity increases sharply from 32.9 to 34.2 and decreases gradually to 32.7. These hydrography-based SST gradients are comparable to the satellite-based values in winter, when temperature fronts are the strongest [Wang *et al.*, 2001; Chang *et al.*, 2006, 2010]. In addition, the satellite SST and its detected front maps (Figures 14.12(c) and 14.12(d)) also clearly indicate the cold region over the Taiwan Bank and the TBF.

The non-monotonic temperature change across the TBF suggests that it could be divided into two parts: the southern part, TS, and the northern part, TN. This north–south structure of TBF could also be identified by the salinity values. The south–north asymmetry of the TBF was also evident from other hydrographic and satellite data (not shown).

14.6.2 *Southwest coastal upwelling front*

The summertime southwest coastal upwelling front (SCUF) has been reported in previous studies based on hydrographic observations, but

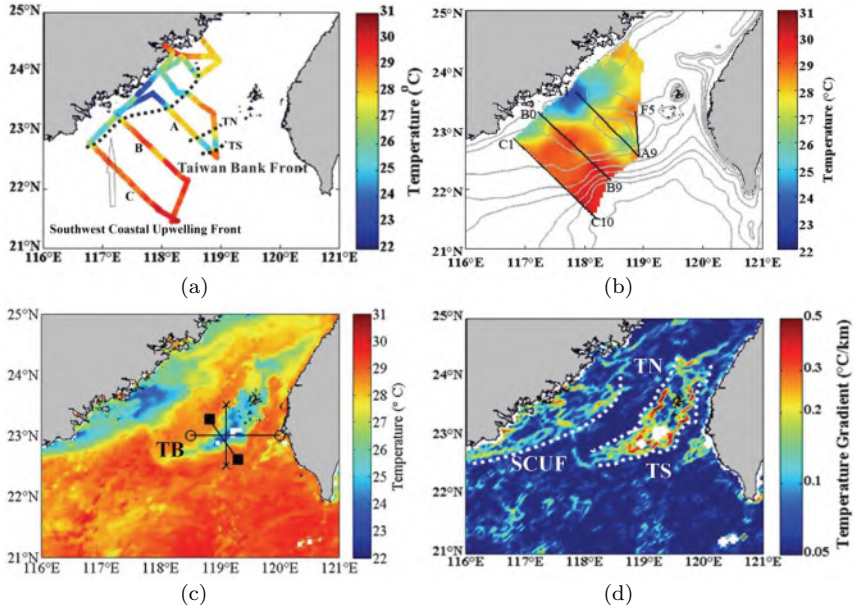

Fig. 14.12. (a) Continuously measured underway surface temperature along the cruise track during the summer cruise from 30 June to 4 July 2011; (b) interpolated surface temperature from (a); (c) the composite SST from daily satellite observations during 30 June–4 July 2011 and (d) the frontal map (log-transformed magnitude of SST gradient) computed from (c).

Notes: A, B and C in (a) denote hydrographic transects A1–A9, B0–B9 and C1–C10, respectively; TN and TS are northern and southern parts of the Taiwan Bank Front (TBF). TB and SCUF are Taiwan Bank and Southwest Coastal Upwelling Front, respectively. In (b), gray contours are isobaths and black lines are cruise transects. Dashed lines in (a) and (d) delineate the approximate locations of SCUF and partial TBF (TS and TN).

Source: From Zhang *et al.* [2014].

mainly identified along single hydrographic transects [Tang *et al*., 2002; Gan *et al*., 2009]. Zhang *et al.* [2014] investigated the SCUF from both hydrographic and satellite observations.

The SCUF appears in all cross-front transects (A, B and C in Figure 14.12(a)). Along transect A, temperature increases from 23.5°C to 27.7°C within 20 km (from A2 to A3), representing a frontal gradient of 0.21°C/km (see [Zhang *et al*., 2014; Figure 6]). Temperature increases are also seen in transects B and C, where the SCUF has frontal widths of 8 and 17 km, with frontal gradients of 0.44°C/km and 0.14°C/km, respectively (see [Zhang *et al*., 2014; Figure 7]). Meanwhile, the salinity front formed by the Pearl River Plume Extension (PRPE) water and the coastal

upwelling water closely follows the temperature front. The salinity frontal gradients for transects A, B and C are 0.07, 0.05 and 0.17 km^{-1}, respectively.

The SCUF is also detected from satellite data. The summertime coastal upwelling induces a large patch of low-SST area along the southwest coast of the Taiwan Strait (Figure 14.12(c)). A prominent SST front (i.e., SCUF) is discerned given the coastal upwelled cold water and the offshore warm water. The SCUF is located along the periphery of the coastal upwelling. Note that the log-transformed SST gradient brings out both the strong TBF and the relatively weak SCUF.

Compared to the TBF, the SCUF is different in two aspects: first, the SCUF is much weaker than the TBF (Figure 14.12(d)); second, the SCUF displays significant spatial differences along the coastal upwelling periphery (Figure 14.12(d)).

14.6.3 *Pearl River plume extension front (PRPEF)*

The extension of the low-salinity water originated from the Pearl River Estuary has been intensively studied by previous investigators [Gan *et al.*, 2009; Ou *et al.*, 2009]. The extended low-salinity water is referred to as the PRPE water hereafter.

Hydrographic data indicate that the PRPE water could reach as far as the Taiwan Bank (Figure 14.13). Zhang *et al.* [2014] also point out that the PRPE water expands in width and shifts offshore as it extends eastward to the southern Taiwan Strait. These observations are consistent with previous studies [Gan *et al.*, 2009].

Two salinity fronts form on the northern and southern flanks of the PRPE water as shown in Figure 14.13. The relatively fresh PRPE water and salty upwelled water generate the salinity front on the northern side, which is also the salinity aspect of the SCUF, coinciding with the temperature aspect (not shown). On the southern side, the temperature of the PRPE water is similar to the surrounding water before it reaches the Taiwan Bank, so the PRPEF is mainly a salinity front.

The PRPE is relatively narrow ($\sim$30 km) and fresh ($\sim$29.7 PSU) along transect C. Consequently, both SCUF and PRPEF are much stronger along transect C than those along transects A and B. The salinity gradient magnitudes of SCUF and PRPEF along transect C are 0.17 and 0.15 km^{-1}, with widths of 18 and 22 km, respectively. As the PRPE water extends northeastward, it gets widened and weakened, leading to weakened PRPEF in

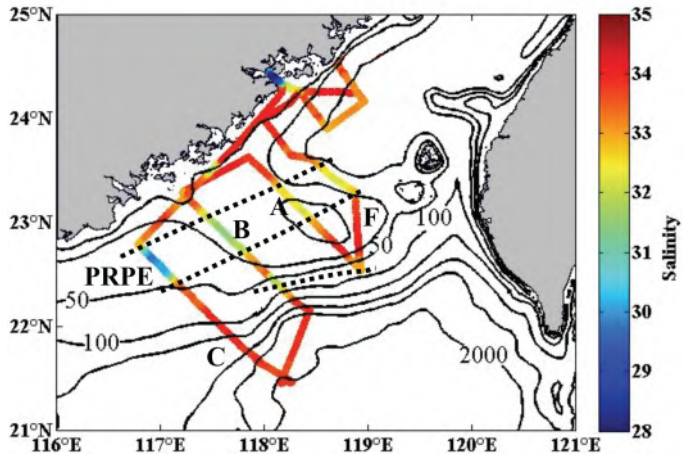

Fig. 14.13. Surface salinity continuously measured underway along the cruise track.

Notes: A, B, C and F denote hydrographic transects A1–A9, B0–B9, C1–C10 and A9–F5, respectively. The dashed lines delineate the Pearl River Plume Extension (PRPE) water and its bifurcation. The bathymetry is superimposed (black contours).

Source: From Zhang *et al.* [2014].

transects A and B. Along transect A, frontal salinity gradients for SCUF and PRPEF are 0.07 and 0.04 km^{-1}, with frontal widths of 15 and 52 km, respectively. Along transect B, frontal salinity gradients are 0.05 and 0.06 km^{-1}, with frontal widths of 40 and 21 km, respectively. These measurements are in good agreement with previous results [Hu *et al.*, 2011].

14.7 Summary

This chapter reviews representative studies regarding the long front band along mainland China. The southern part of the front band highlights the existence of surface Chl-a and SST fronts around the Hainan Island and in the Beibu Gulf by Hu *et al.* [2003]. They suggest that tidal mixing plays a key role in forming surface Chl-a fronts, but less so for SST fronts. The central part of the front band, mostly the Guangdong coastal fronts, was investigated by Wu *et al.* [2015] using a statistical modeling approach specifically optimized for that region. The temperature range and width of fronts extracted from that approach contribute to a more comprehensive view of the frontal system in the NSCS. The northern part of the front band mostly concerns fronts in the Taiwan Strait. Their magnitudes peak

during winter and spring, decay and reach the minimum during summer, and increase again during autumn [Pi and Hu, 2010]. During winter, fine-scale structure of SST fronts in the Taiwan Strait is reported by Li *et al.* [2006] using satellite SST images, which feature complex geometry due to interleaving of cold and warm water masses of different origins. Their vessel-based observations confirm some of the findings from satellite images, and further reveal vertical structures of those fronts. Zhang *et al.* [2014], on the other hand, present a detailed description of summertime fronts in the Taiwan Strait, i.e., TBF, SCUF and PRPEF, with surface temperature and salinity changes across those fronts being quantified.

Acknowledgments

This study is jointly supported by the National Basic Research Program of China (2015CB954004) and the National Natural Science Foundation of China (No. 91958203, 41606009, 41776027 and U1405233), Xiamen University Fundamental Research Funds for the Central Universities (20720180099), and Laboratory for Regional Oceanography and Numerical Modeling, Pilot National Laboratory for Marine Science and Technology (Qingdao) (No. 2017A02).

References

Belkin, I. M., Cornillon, P. C. and Sherman, K. (2009). Fronts in large marine ecosystems, *Prog. Oceanogr.*, 81, pp. 223–236.

Cayula, J.-F. and Cornillon, P. (1995). Multi-image edge detection for SST images, *J. Atmos. Oceanol. Technol.*, 12, pp. 821–829.

Chang, Y., Shieh, W., Lee, M., Chan, J., Lan, K., and Weng, J., (2010). Fine-scale sea surface temperature fronts in wintertime in the northern South China Sea, *Int. J. Remote Sens.*, 31 (17–18), pp. 4807–4818.

Chang, Y., Shimada, T., Lee, M.-A., Lu, H.-J., Sakaida, F. and Kawamura, H. (2006). Wintertime sea surface temperature fronts in the Taiwan Strait, *Geophys. Res. Lett.*, 33, L23603.

Fang, G., Kwok, Y.-K., Yu, K. and Zhu, Y. (1999). Numerical simulation of principal tidal constituents in the South China Sea, Gulf of Tonkin and Gulf of Thailand, *Cont. Shelf Res.*, 19, pp. 845–869.

Ferrari, R. (2011). A frontal challenge for climate models, *Science*, 332 (6072), pp. 316–317.

Gan, J., Li, L., Wang, D. and Guo, X. (2009). Interaction of a river plume with coastal upwelling in the northeastern South China Sea, *Cont. Shelf Res.*, 29, pp. 728–740.

Hickox, R., Belkin, I.M., Cornillon, P., Shan, Z., (2000). Climatology and seasonal variability of ocean fronts in the East China, Yellow and Bohai Seas from satellite SST data, *Geophys. Res. Lett.*, 27 (18), pp. 2945–2948.

Hopkins, J., Challenor, P. and Shaw, A. G. P. (2010). A new statistical modeling approach to ocean front detection from SST satellite images, *J. Atmos. Ocean. Technol.*, 27, pp. 173–191.

Hu, J., Hong, H., Li, Y., Jiang, Y., Chen, Z., Zhu, J., Wan, Z., Sun, Z. and Liang, H. (2011). Variable temperature, salinity and water mass structures in the southwestern Taiwan Strait in summer, *Cont. Shelf Res.*, 31, pp. S13–S23.

Hu, J., Kawamura, H. and Tang, D. (2003). Tidal front around the Hainan Island, northwest of the South China Sea, *J. Geophys. Res.*, 108 (C11), pp. 3342 6:1–9.

Hu, J., Kawamura, H., Hong, H., Kobashi, F. and Xie, Q. (2001). Tidal features in the China Seas and their adjacent sea areas as derived from TOPEX/POSEIDON altimeter data, *Chin. J. Oceanol. Limnol.*, 19, pp. 293–305.

Hu, J., Kawamura, H., Li, C., Hong, H. and Jiang, Y. (2010). Review on current and seawater volume transport through the Taiwan Strait, *J. Oceanogr.*, 66, pp. 591–610.

Huang, Q. Z., Wang, W. Z. and Chen, J. C. (1994). Tides, tidal currents and storm surge set-up of South China Sea, in Z. Di, L. Yan-Bo, Z. Cheng-Kui (Eds.), Oceanology of China Sea, Vol. 1, pp. 113–122. Springer, Dordrecht.

Jan, S., Wang, J., Chern, C.-S. and Chao, S.-Y. (2002). Seasonal variation of the circulation in the Taiwan Strait, *J. Mar. Syst.*, 35, pp. 249–268.

Jing, Z., Qi, Y., Du, Y., Zhang, S. and Xie, L. (2015). Summer upwelling and thermal fronts in the northwestern South China Sea: Observational analysis of two mesoscale mapping surveys, *J. Geophys. Res. Oceans*, 120, pp. 1993–2006.

Li, C., Hu, J., Jan, S., Wei, Z., Fang, G. and Zheng, Q. (2006). Winter-spring fronts in Taiwan Strait, *J. Geophys. Res.*, 111, C11S13.

Loder, J. W. and Greenberg, D. A. (1986). Predicted positions of tidal fronts in the Gulf of Maine region, *Cont. Shelf Res.*, 6, pp. 397–414.

Ou, S., Zhang, H. and Wang, D. (2009). Dynamics of the buoyant plume off the Pearl River Estuary in summer, *Environ. Fluid Mech.*, 9, pp. 471–492.

Pi, Q. and Hu, J. (2010). Analysis of sea surface temperature fronts in the Taiwan Strait and its adjacent area using an advanced edge detection method, *Sci. China Earth Sci.*, 53, pp. 1008–1016.

Qiu, C., Cui, Y., Hu, S. and Dan, H. (2017). Seasonal variation of Guangdong coastal thermal front based on merged satellite data, *J. Trop. Oceanogr.*, 36, pp. 16–23 (in Chinese with English abstract).

Shimada, T., Sakaida, F., Kawamura, H. and Okumura, T. (2005). Application of an edge detection method to satellite images for distinguishing sea surface temperature fronts near the Japanese coast, *Remote Sens. Environ.*, 98, pp. 21–34.

Simpson, J. H. and Hunter, J. R. (1974). Fronts in the Irish Sea, *Nature*, 250, pp. 404–406.

Tang, D., Kawamura, H., Lee, M.-A., and Tran, V. D. (2003). Seasonal and spatial distribution of chlorophyll-a concentrations and water conditions in the Gulf of Tonkin, South China Sea, *Remote Sens. Environ.*, 85, pp. 475–483.

Tang, D., Kester, D., Ni, I., Kawamura, H. and Hong, H. (2002). Upwelling in the Taiwan Strait during the summer monsoon detected by satellite and shipboard measurements, *Remote Sens. Environ*., 83, pp. 457–471.

Taylor, J. R. and Ferrari, R. (2011). Ocean fronts trigger high latitude phytoplankton blooms, *Geophys. Res. Lett*., 38 (23), 23601.

Vázquez, D. P., Atae-Allah, C. and Escamilla, P. L. L. (1999). Entropic approach to edge detection for SST images, *J. Atmos. Ocean. Technol*., 16, pp. 970–979.

Wang. L. (2004). *A Study of Fronts and Frontal Eddies in the Northern Shelf Region of the South China Sea*, master thesis, Ocean University of China.

Wang, D., Liu, Y., Qi, Y. and Shi, P. (2001). Seasonal variability of thermal fronts in the northern South China Sea from satellite data, *Geophys. Res. Lett*., 28, pp. 3963–3966.

Wu, Q., Hu, J., Sun, Z. and Zhu, J. (2015). Improvement and validation of a statistical modeling approach to ocean front detection, *J. Xiamen Univ. Nat. Sci*., 54 (2), pp. 199–206 (in Chinese with English abstract).

Xie, L., Pallàs-Sanz, E., Zheng, Q., Zhang, S., Zong, X., Yi, X. and Li, M. (2017). Diagnosis of 3D vertical circulation in the upwelling and frontal zones east of Hainan Island, China, *J. Phys. Oceanogr*., 47 (4), pp. 755–774.

Yanagi, T., Takao, T. and Morimoto, A. (1997). Co-tidal and co-range charts in the South China Sea derived from satellite altimetry data, *La mer*, 35, pp. 85–93.

Zhang, F., Li, X., Hu, J., Sun, Z., Zhu, J. and Chen, Z. (2014). Summertime sea surface temperature and salinity fronts in the southern Taiwan strait, *Int. J. Remote Sens.*, 35 (11–12), pp. 4452–4466.